

Molecular Dynamics Simulation of Nanoindentation-induced Mechanical Deformation and Phase Transformation in Monocrystalline Silicon

Yen-Hung Lin · Sheng-Rui Jian · Yi-Shao Lai ·
Ping-Feng Yang

Received: 2 December 2007 / Accepted: 11 January 2008 / Published online: 25 January 2008
© to the authors 2008

Abstract This work presents the molecular dynamics approach toward mechanical deformation and phase transformation mechanisms of monocrystalline Si(100) subjected to nanoindentation. We demonstrate phase distributions during loading and unloading stages of both spherical and Berkovich nanoindentations. By searching the presence of the fifth neighboring atom within a non-bonding length, Si-III and Si-XII have been successfully distinguished from Si-I. Crystallinity of this mixed-phase was further identified by radial distribution functions.

Keywords Monocrystalline silicon · Nanoindentation · Molecular dynamics · Phase transformation

Introduction

Silicon plays an important role in applications such as semiconductor devices, sensors, mechanical elements, and electronics. Its electronic characteristics have therefore been intensively investigated. Mechanical properties of Si, however, became a research focus only in the past few years owing to the development of the silicon on insulator

(SOI) technology and microelectromechanical systems (MEMS), in which Si serves as a substrate. For these applications, deformation mechanisms of Si under nano-contact are essential.

It is well-known that diamond cubic Si (Si-I) undergoes pressure-induced phase transformations during mechanical loading using diamond anvil cell (DAC) or nanoindentation [1–6]. The Si-I transforms to the metallic β -Sn (Si-II) phase under a load of up to 11 GPa [1]. Upon pressure release, Si-II undergoes a further phase transformation to a mixed-phase of Si-III (bc8, body-centered-cubic structure) and Si-XII (r8, rhombohedral structure) at a low unloading rate while it transforms to the α -Si phase at a fast unloading rate [3, 7, 8]. Jang et al. [9] reported the extrusion and phase change mechanism using a sharp or blunt indenter with various indentation loads and rates. Phase transformations corresponding to repeated indentations were also studied by Zarudi et al. [10, 11].

Comprehensive understanding of phase transformations in Si requires the use of experimental techniques such as cross-sectional transmission electron microscopy (XTEM), scanning electron microscopy (SEM), and Raman microspectroscopy [5, 10]. On the other hand, molecular dynamics (MD) simulations have also been employed to identify the phase transformation mechanism. Among related MD studies, Cheong and Zhang [12] identified different phases through their coordination numbers and also performed the radial distribution function (RDF) analysis. A stress criterion for the onset of the transformation to Si-II was also proposed [13, 14].

This study presents the MD approach toward mechanical deformation and phase transformation mechanisms of monocrystalline Si(100) subjected to nanoindentation. The MD simulations were performed to identify load-displacement characteristics of the nanoindentation process

Y.-H. Lin
Department of Mechanical Engineering, National Cheng Kung University, Tainan 701, Taiwan, ROC

S.-R. Jian
Department of Materials Science and Engineering,
I-Shou University, Kaohsiung 840, Taiwan, ROC

Y.-S. Lai (✉) · P.-F. Yang
Central Labs, Advanced Semiconductor Engineering, Inc.,
26 Chin 3rd Rd., Nantze Export Processing Zone,
Kaohsiung 811, Taiwan, ROC
e-mail: yishao_lai@aseglobal.com

and nanoindentation-induced phase transformations during loading and unloading. Both spherical and Berkovich indenters were considered.

Molecular Dynamics Simulation

The interatomic potential function proposed by Tersoff [15–18] that considers the effect of bond angle and covalent bonds has been shown to be particularly feasible in dealing with IV elements and those with a diamond lattice structure such as carbon, silicon, and germanium. The Tersoff function was therefore adopted in this study to analyze the dynamic correlations in carbon–carbon and silicon–silicon atoms. In regard to the mutual interaction between carbon and silicon under the equivalent potential, we made use of the two-body Morse potential [12], which has been well described for carbon–silicon atoms. Although a two-body potential leads to less precise solutions than a many-body potential does, its parameters can be accurately calibrated by spectrum data, and hence is extensively employed in MD simulations. In addition to the periodic boundary conditions, a modified five-step methodology was used to incorporate Newton's equations of motion so that the position and velocity of a particle can be effectively evaluated. Moreover, the mixed neighbor list was applied to enhance computational efficiency.

Physical models for spherical and Berkovich indenters contained 46,665 and 29,935 carbon atoms, respectively, with covalent bonds. The $250 \text{ \AA} \times 250 \text{ \AA} \times 175 \text{ \AA}$ modeling region of the (001)-oriented Si substrate contained 518,400 silicon atoms with covalent bonds. We simulated the nanoindentation process by applying perpendicular loading along the (001) direction. Detailed MD modeling and calculation techniques of nanoindentation on monocrystalline Si(100) are referred to Lin et al. [19]. The maximum penetration depth in the present MD simulations was set at 3.5 nm.

Results and Discussion

Since the formation of metastable Si-III and Si-XII phases is strongly stress-dependent, different stress distributions induced by spherical and Berkovich indenters would result in different Si-III and Si-XII distributions within the nanoindentation-induced deformed region. Boyer et al. [20] have observed and discussed the presence of Si-I, Si-II, Si-III, Si-XII, and bct5-Si phases during nanoindentation. Among the several possible mechanisms of phase transformations in Si, it is generally acceptable that Si-I transforms to the metallic Si-II during the loading stage. The Si-I crystalline structure contains four nearest

neighbors at a distance of 2.35 \AA at ambient pressure. When the stress increases up to 10.3 GPa, Si-I transforms to Si-II, whose crystalline structure contains four nearest neighbors at a distance of 2.42 \AA along with two others at 2.57 \AA . Moreover, the bct5-Si crystalline structure contains one neighbor at a distance of 2.31 \AA and four others at 2.44 \AA [21]. The Si-III is constructed by four nearest neighbors within a distance of 2.37 \AA and a unique one at 3.41 \AA at 2 GPa. The Si-XII is with the four nearest neighbors within a distance of 2.39 \AA and also a unique one at a distance of 3.23 or 3.36 \AA at 2 GPa [22, 23]. Upon pressure release, part of the highly pressured Si-II phase would transform to a mixed-phase of metastable Si-III and Si-XII. Although distinguishing of Si-III and Si-XII from Si-I apparently has been a difficulty in previous MD studies because the coordination numbers of these phases are identical at four, the two metastable phases can be readily identified from Si-I by searching the presence of the fifth neighboring atom within a non-bonding length.

Previous MD simulations showed that under nanoindentation, the bond angle along the (001)-oriented surface direction of monocrystalline Si could be gradually compressed from 90° to 70° , whereas the relative slip among atoms along the compression direction would slowly form Si-II [24]. A pop-in event encountered during the loading stage is an indicator of the occurrence of plastic deformation that leads to phase transformation from Si-I to Si-II in the severely compressed region [19]. Most of the previous studies that explored phase transformations of Si applied a spherical indenter capable of triggering large-scale phase transformations. In the present MD simulations, a spherical indenter was first adopted to interpret phase transformation features in monocrystalline Si. We then adopted a Berkovich indenter in the simulations to compare the difference of phases induced by the two indenters.

Figure 1 shows the load–displacement curves led by spherical and Berkovich indenters. At an identical penetration depth, the total deformation energy of the spherical indenter is larger than that of the Berkovich indenter. An apparent pop-out event is also present for the spherical indenter during the unloading stage. However, the pop-out event is unapparent for the Berkovich indenter perhaps because the maximum penetration depth is not large enough in the MD simulations to trigger the event.

Figure 2a shows phase distributions on the cross-sectional (011) plane under an indentation load induced by the spherical indenter along (001) at the moment when the maximum penetration depth is reached. Clearly, the highly pressured zone (in red) is surrounded from below by the Si-II phase (in yellow) while the Si-II phase is surrounded by the bct5-Si phase (in cyan). The tilted distributions of these phases follow the {110} slip planes of monocrystalline Si. It is particularly interesting to note that a ring

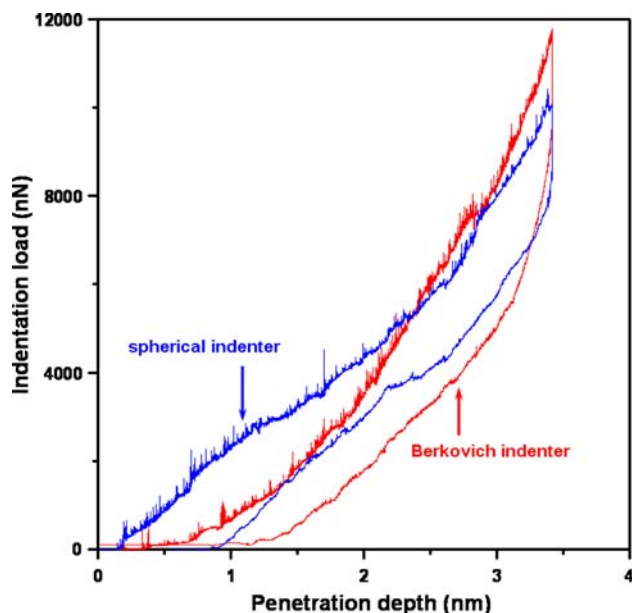


Fig. 1 MD simulations of load–displacement curves for monocrystalline Si(100) led by spherical and Berkovich indenters at room temperature

representing a mixed-phase of bct5-Si and Si-I (blank) is present close to the boundary of Si-II. The presence of this mixed-phase implies that energy transfer during nanoindentation is non-continuous, indicating that the continuum assumption is no longer feasible under such a circumstance. Figure 2b shows phase distributions on the cross-sectional (011) plane after the spherical indenter is completely withdrawn. Residual phases consist of a mixture of Si-III and Si-XII (in green), Si-II, and the amorphous phase. The presence of Si-III and Si-XII as well as the amorphous phase corresponds to the pop-out event occurred during the unloading stage. Furthermore, recrystallization upon unloading is the most active along the slip planes.

Phase distributions on the cross-sectional (011) plane induced by a Berkovich indenter, as shown in Fig. 3, are in general similar to the ones induced by a spherical indenter, while the phase transformation region of the former is smaller than the latter. A ring surrounding Si-II of a mixed-phase of bct5-Si and Si-I is also present.

Crystallinity of Si-III and Si-XII for monocrystalline Si(100) subjected to spherical or Berkovich indentation along the (001) direction was identified by RDF, as shown in Fig. 4. For both indentations, there are obvious peaks at bond lengths of 2.3–2.4 Å, 3 Å, and 3.2–3.45 Å. The first peak corresponds to the fact that the mixed-phase of Si-III and Si-XII is concentrated at 2.37–2.39 Å while the third peak refers to the presence of the fifth neighboring atom of Si-III or Si-XII within a non-bonding length at 3.23–3.41 Å. The second peak at 3 Å should come from the

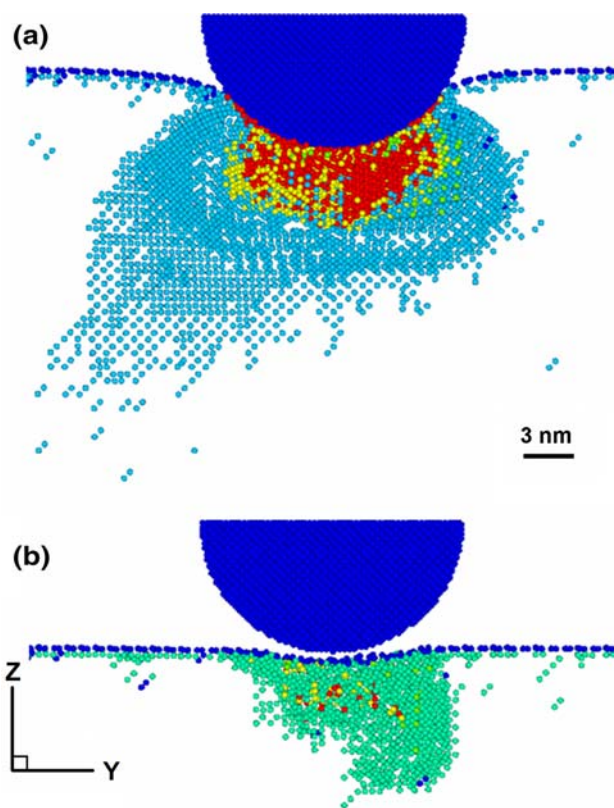


Fig. 2 Cross-sectional views on (011) plane of phase transformation regions in monocrystalline Si(100) led by spherical indenter: (a) maximum penetration depth at 3.5 nm; (b) completely withdrawn

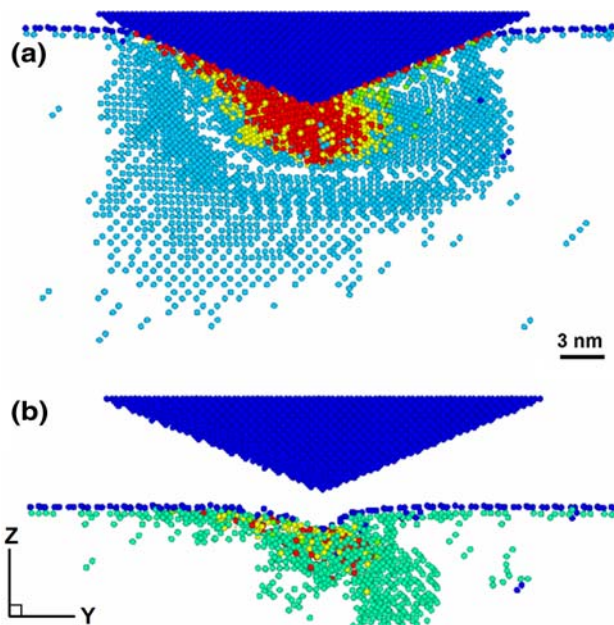


Fig. 3 Cross-sectional views on (011) plane of phase transformation regions in monocrystalline Si(100) led by Berkovich indenter: (a) maximum penetration depth at 3.5 nm; (b) completely withdrawn

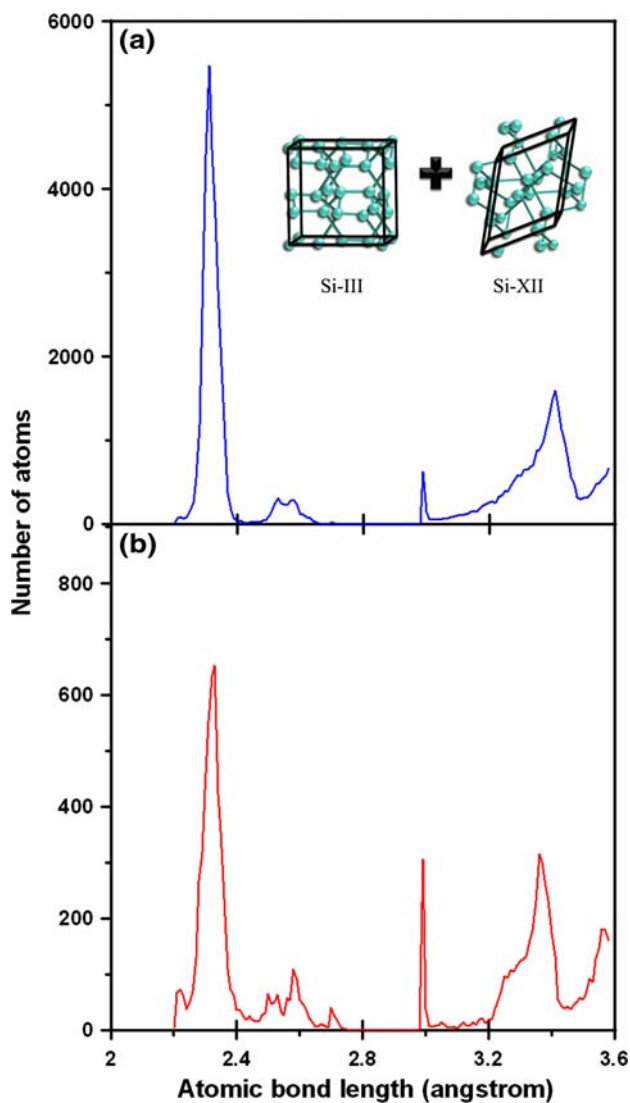


Fig. 4 RDF of bond length for Si-III and Si-XII by (a) spherical and (b) Berkovich indenters

amorphous phase [25] whose atoms are separated at the critical bond length set in our MD simulations (3 Å) as a result of atomic interactions between the indenter and Si. We need to emphasize that this particular peak would correspond to a slightly different bond length when a different potential function is followed. Moreover, minor peaks at bond lengths greater than 3 Å can be referred to thermal vibrations of Si atoms [25].

Conclusion

Nanoindentation-induced deformation and phase transformations in monocrystalline Si(100) were investigated through MD simulations. The Si-III and Si-XII were distinguished from Si-I by searching the presence of the fifth neighboring atom within a non-bonding length. Crystallinity

of the mixed Si-III and Si-XII phase was further identified by RDF. The MD results also indicate that phase distributions induced by a Berkovich indenter are in general similar to the ones induced by a spherical indenter, while the phase transformation region of the former is smaller than the latter.

Acknowledgment This work was supported in part by National Science Council of Taiwan through Grants NSC 94-2212-E-006-048 and NSC 96-2112-M-214-001.

References

1. D.R. Clarke, M.C. Kroll, P.D. Kirchner, R.F. Cook, B.J. Hockey, Amorphization and conductivity of silicon and germanium induced by indentation. *Phys. Rev. Lett.* **60**(21), 2156–2159 (1988)
2. Y.Q. Wu, X.Y. Yang, Y.B. Xu, Cross-sectional electron microscopy observation on the amorphized indentation region in [001] single-crystal silicon. *Acta Mater.* **47**(80), 2431–2436 (1999)
3. V. Domnich, Y. Gogotsi, S. Dub, Effect of phase transformations on the shape of the unloading curve in the nanoindentation of silicon. *Appl. Phys. Lett.* **76**(16), 2214–2216 (2000)
4. A.B. Mann, D. van Heerden, J.B. Pethica, T.P. Weihs, Size-dependent phase transformations during point loading of silicon. *J. Mater. Res.* **15**(8), 1754–1758 (2000)
5. J.E. Bradby, J.S. Williams, J. Wong-Leung, M.V. Swain, P. Munroe, Mechanical deformation in silicon by micro-indentation. *J. Mater. Res.* **16**(5), 1500–1507 (2001)
6. T. Juliano, Y. Gogotsi, V. Domnich, Effect of indentation unloading conditions on phase transformation induced events in silicon. *J. Mater. Res.* **18**(5), 1192–1201 (2003)
7. A. Kailer, Y.G. Gogotsi, K.G. Nickel, Phase transformations of silicon caused by contact loading. *J. Appl. Phys.* **81**(7), 3057–3063 (1997)
8. R.O. Piltz, J.R. Maclean, S.J. Clark, G.J. Ackland, P.D. Hatton, J. Crain, Structure and properties of silicon XII: a complex tetrahedrally bonded phase. *Phys. Rev. B* **52**(6), 4072–4085 (1995)
9. J.-I. Jang, M.J. Lance, S. Wen, T.Y. Tsui, G.M. Pharr, Indentation-induced phase transformations in silicon: influences of load, rate and indenter angle on the transformation behavior. *Acta Mater.* **53**(6), 1759–1770 (2005)
10. I. Zarudi, L.C. Zhang, M.V. Swain, Microstructure evolution in monocrystalline silicon in cyclic microindentations. *J. Mater. Res.* **18**(4), 758–761 (2003)
11. I. Zarudi, L.C. Zhang, M.V. Swain, Behavior of monocrystalline silicon under cyclic microindentations with a spherical indenter. *Appl. Phys. Lett.* **82**(7), 1027–1029 (2003)
12. W.C.D. Cheong, L.C. Zhang, Molecular dynamics simulation of phase transformations in silicon monocrystals due to nano-indentation. *Nanotechnology* **11**(3), 173–180 (2000)
13. W.C.D. Cheong, L.C. Zhang, A stress criterion for the β -Sn transformation in silicon under indentation and uniaxial compression. *Key Eng. Mater.* **233–236**, 603–608 (2003)
14. I. Zarudi, L.C. Zhang, W.C.D. Cheong, T.X. Yu, The difference of phase distributions in silicon after indentation with Berkovich and spherical indenters. *Acta Mater.* **53**(18), 4795–4800 (2005)
15. J. Tersoff, New empirical model for the structural properties of silicon. *Phys. Rev. Lett.* **56**(6), 632–635 (1986)
16. J. Tersoff, New empirical approach for the structure and energy of covalent systems. *Phys. Rev. B* **37**(12), 6991–7000 (1988)
17. J. Tersoff, Empirical interatomic potential for silicon with improved elastic properties. *Phys. Rev. B* **38**(14), 9902–9905 (1988)

18. J. Tersoff, Modeling solid-state chemistry: interatomic potentials for multicomponent systems. *Phys. Rev. B* **39**(8), 5566–5568 (1989)
19. Y.-H. Lin, T.-C. Chen, P.-F. Yang, S.-R. Jian, Y.-S. Lai, Atomic-level simulations of nanoindentation-induced phase transformation in mono-crystalline silicon. *Appl. Surf. Sci.* **254**(5), 1415–1422 (2007)
20. L.L. Boyer, E. Kaxiras, J.L. Feldman, J.Q. Broughton, M.J. Mehl, New low-energy crystal structure for silicon. *Phys. Rev. Lett.* **67**(6), 715–718 (1991)
21. D.E. Kim, S.I. Oh, Atomistic simulation of structural phase transformations in monocrystalline silicon induced by nanoindentation. *Nanotechnology* **17**(9), 2259–2265 (2006)
22. J. Crain, S.J. Clark, G.J. Ackland, M.C. Payne, V. Milman, P.D. Hatton, B.J. Reid, Theoretical study of high-density phases of covalent semiconductors. I. *Ab initio* treatment. *Phys. Rev. B* **49**(8), 5329–5340 (1994)
23. J. Crain, G.J. Ackland, J.R. Maclean, R.O. Piltz, P.D. Hatton, G.S. Pawley, Reversible pressure-induced structural transitions between metastable phases of silicon. *Phys. Rev. B* **50**(17), 13043–13046 (1994)
24. F. Shimojo, I. Ebbsjö, R.K. Kalia, A. Nakano, J.P. Rino, P. Vashishta, Molecular dynamics simulation of structural transformation in silicon carbide under pressure. *Phys. Rev. Lett.* **84**(15), 3338–3341 (2000)
25. C.F. Sanz-Navarro, S.D. Kenny, R. Smith, Atomistic simulations of structural transformations of silicon surfaces under nanoindentation. *Nanotechnology* **15**(5), 692–697 (2004)